

Consequences of Triaxiality for Gravitational Wave Recoil of black holes

Alessandro Vicari,¹ Roberto Capuzzo-Dolcetta,¹ David Merritt²

¹*Dipartimento di Fisica, Universita' di Roma La Sapienza P.le A.Moro 5, I-00185, Roma, Italy;*

²*Department of Physics, Rochester Institute of Technology, 85 Lomb Memorial Drive, Rochester, NY 14623, USA*

ABSTRACT

Coalescing binary black holes experience a “kick” due to anisotropic emission of gravitational waves with an amplitude as great as $\sim 200 \text{ km s}^{-1}$. We examine the orbital evolution of black holes that have been kicked from the centers of triaxial galaxies. Time scales for orbital decay are generally longer in triaxial galaxies than in equivalent spherical galaxies, since a kicked black hole does not return directly through the dense center where the dynamical friction force is highest. We evaluate this effect by constructing self-consistent triaxial models and integrating the trajectories of massive particles after they are ejected from the center; the dynamical friction force is computed directly from the velocity dispersion tensor of the self-consistent model. We find return times that are several times longer than in a spherical galaxy with the same radial density profile, particularly in galaxy models with dense centers, implying a substantially greater probability of finding an off-center black hole.

Subject headings: black hole physics - galaxies: nuclei - galaxies: bulges - galaxies: kinematics and dynamics - galaxies: elliptical and lenticular, CD

1. Introduction

The coalescence of binary black holes (BHs) results in a gravitational recoil, or “kick”, due to the net linear momentum carried away by gravitational waves. Bekenstein (1973) estimated a kick velocity $V \approx 300 \text{ km s}^{-1}$ in highly nonspherical collapses using a quasi-Newtonian formalism. Nakamura et al. (1987) computed $V/c = 0.045\eta^2$ for head-on collisions from infinity using BH perturbation theory; here $\eta \equiv \mu/(M_1 + M_2)$, the “reduced mass ratio”, with M_1, M_2 the BH masses and $\mu \equiv M_1 M_2 / (M_1 + M_2)$ the reduced mass. A number of analytic estimates have been made of V for circular-orbit inspirals (Fitchett 1983; Fitchett & Detweiler 1984; Wiseman 1992; Favata, Hughes & Holz 2004). The kick amplitude is usually divided into two components: the net recoil up to the innermost stable

circular orbit (ISCO), and the contribution from the final plunge, from the ISCO to the horizon, which takes place in the strong-field regime and which dominates the total kick. Blanchet, Qusailah & Will (2005) computed V to second post-Newtonian order and found it to be well approximated by the simple formula

$$\frac{V}{c} = 0.043\eta^2 \sqrt{1 - 4\eta} \left(1 + \frac{\eta}{4}\right). \quad (1)$$

The $\eta^2(1 - 4\eta)^{1/2}$ dependence is the same found by Fitchett (1983), who computed gravitational recoil for a pair of BHs interacting via Newtonian forces and included only the lowest gravitational wave multipoles needed for momentum ejection. With the additional, ad hoc factor in equation (1), Blanchet, Qusailah & Will (2005) were able to reproduce the results of their 2PN calculations to better than 1% at all mass ratios.

In the last year, remarkable progress has been made in techniques for the numerical solution of the full field equations (Pretorius 2005, 2006; Campanelli et al. 2005; Campanelli, Kelly & Lousto 2006; Baker et al. 2006a,b) allowing several groups to compute recoil velocities for coalescing BH binaries without approximations. Baker et al. (2006c) find $V = 105 \pm 10 \text{ km s}^{-1}$ for $M_2/M_1 = 2/3$. Herrmann, Shoemaker & Laguna (2006) derive $V = 33 \text{ km s}^{-1}$ for $M_2/M_1 = 0.85$ and $V = 9 \text{ km s}^{-1}$ for $M_2/M_1 = 0.96$. Most recently, González et al. (2006) carried out a large set of inspiral simulations for non-spinning, circular-orbit binaries and determined the kick velocity as a function of mass ratio. Their results are well described by the expression

$$\frac{V}{c} = 0.040\eta^2 \sqrt{1 - 4\eta} (1 - 0.93\eta), \quad (2)$$

implying a maximum kick velocity of 175.7 km s^{-1} at $M_2/M_1 = 0.36$, somewhat smaller than implied by equation (1). The dependence of the kick velocity on orbital eccentricity was investigated by Sopuerta, Yunes and Laguna (2006) using the close-limit approximation, which models the late stages of coalescence as a single perturbed BH, coupled with a post-Newtonian estimate of the recoil during the early evolution. Their results are consistent with a $(1 + e)$ dependence of kick velocity on eccentricity for the low ($e \leq 0.1$) eccentricities which they investigated, i.e. $V \approx 195 \text{ km s}^{-1}$ for $e = 0.1$.

All of these results were obtained for non-spinning holes. In the presence of spin, kick velocities might be larger and would be nonzero even for $M_1 = M_2$ (Redmount & Rees 1989; Favata et al. 2004). Calculations of the coalescence of spinning BHs are currently underway (Campanelli, Lousto and Zlochower 2006a, b).

In this paper, we consider some of the consequences of the kicks for supermassive BHs in galactic nuclei. A kick velocity of 200 km s^{-1} is sufficient to remove a coalesced BH from a dwarf elliptical galaxy, even if the latter is embedded in a dark-matter halo (Merritt et al. 2004). Escape velocities at the centers of luminous elliptical galaxies are generally greater than $\sim 400 \text{ km s}^{-1}$ however, and kicks of the magnitude so far calculated by numerical

relativists would never be expected to remove BHs from such galaxies. But the kicks could still displace the BHs temporarily from their central locations, implying a finite probability of finding an off-center BH in a giant galaxy. The kicks would also generate long-lived changes in the central structure of galaxies as the displaced BHs transfer their orbital energy to the stars via dynamical friction (Merritt et al. 2004; Boylan-Kolchin et al. 2004; Madau & Quataert 2004). The displacements and their side-effects would have been greater at earlier times, when the gravitational potential wells associated with galaxies were shallower (Volonteri et al. 2003; Merritt et al. 2004; Madau & Quataert 2004; Haiman 2004; Yoo & Miralda-Escude 2004; Libeskind et al. 2006).

In a non-spherical galaxy, an ejected BH does not pass precisely through the dense center as it falls back, reducing the mean value of the dynamical friction force compared with a spherical galaxy. The result is a more extended period of displacement compared with estimates based on spherical galaxy models. Here, we evaluate the effect of nonspherical galaxy geometries on BH infall times using fully self-consistent triaxial models. The models are constructed via orbital superposition as in Merritt & Fridman (1996), and the quantities that define the velocity ellipsoid at every point on the solution grid are computed and stored as in Merritt (1980). Given this information, it is possible to compute accurate estimates of the dynamical friction force that would act on a massive object, using the expressions in Pesce, Capuzzo-Dolcetta & Vietri (1992) and Capuzzo-Dolcetta & Vicari (2006). The frictional forces are added to the conservative forces from the triaxial mass distribution when integrating the BH trajectories.

Among the new effects we find here is an increase in the effective “escape velocity” from the center of the galaxy, since some of the BH’s initial kinetic energy is lost to dynamical friction. The kick velocity needed to escape is also dependent on the direction of the kick since the frictional force is direction-dependent. In general, we find that return times are longer in the triaxial geometry by factors of \sim a few compared with return times in spherical galaxies having the same, mean radial density profile, and this translates into a substantially higher probability of finding a displaced BH.

2. Method

A BH ejected from the center of a galaxy moves in response to the conservative force corresponding to the gravitational potential $\Phi(\mathbf{r})$ of the stars and to the dynamical friction force per unit mass $\mathbf{f}_{df}(\mathbf{r})$. Its motion can be approximated by the solution of the differential equation

$$\ddot{\mathbf{r}} = -\nabla\Phi + \mathbf{f}_{df} \quad (3)$$

subject to the proper initial conditions. We assume throughout that neither Φ nor \mathbf{f}_{df} depend explicitly on time.

As usual, we transform this second-order differential equation into a system of first-order equations:

$$\dot{\mathbf{r}} = \mathbf{v}, \quad (4a)$$

$$\dot{\mathbf{v}} = -\nabla\Phi + \mathbf{f}_{df}. \quad (4b)$$

As a consequence of the dynamical friction term, the orbital energy, E , is no longer a conserved quantity. Instead we can write

$$\dot{E} \equiv \dot{E}_{df} = \mathbf{f}_{df} \cdot \mathbf{v} \quad (5)$$

This expression allows us to verify conservation of the total energy $\mathcal{E} = K + \Phi + E_{df}$, where K is the kinetic energy and E_{df} the work done by the dynamical friction force along the trajectory.

We solved the system of differential equations (4) numerically, using the 7/8 order Runge-Kutta algorithm of Fehlberg (1968).¹

2.1. Mass model

We adopted as galaxy models the triaxial generalizations of the spherical Dehnen (1993) models. The mass density is

$$\rho(\mathbf{r}) = \frac{(3-\gamma)M}{4\pi abc} \frac{1}{m^\gamma(1+m)^{4-\gamma}}, \quad 0 \leq \gamma < 3 \quad (6)$$

where

$$m^2 = \frac{x^2}{a^2} + \frac{y^2}{b^2} + \frac{z^2}{c^2}, \quad 0 < c \leq b \leq a \quad (7)$$

and M is the total mass of the galaxy. The gravitational potential generated by this density law is (Chandrasekhar 1969)

$$\Phi(\mathbf{r}) = -\pi Gabc \int_0^\infty \frac{[\psi(\infty)] - \psi(\tilde{m})d\tau}{\sqrt{(\tau+a^2)(\tau+b^2)(\tau+c^2)}} \quad (8)$$

with

$$\psi(\tilde{m}) = \int_0^{\tilde{m}^2} \rho(m'^2) dm'^2, \quad (9)$$

¹The FORTRAN version of this algorithm was kindly made available to us by S. Udry.

$$\psi(\infty) = \lim_{\tilde{m} \rightarrow \infty} \psi(\tilde{m}), \quad (10)$$

and

$$\tilde{m}^2(\tau) = \frac{x^2}{a^2 + \tau} + \frac{y^2}{b^2 + \tau} + \frac{z^2}{c^2 + \tau}. \quad (11)$$

Substituting $s = \sqrt{1 + \tau}$ in equation (8) leads (for $\gamma \neq 2$) to an integral better suited to numerical evaluation (Merritt & Fridman 1996, hereafter MF96):

$$\begin{aligned} \Phi(\mathbf{r}) = & -\frac{1}{\gamma-2} \times \\ & \times \int_0^1 \frac{1-(3-\gamma)(\frac{\tilde{m}}{1+\tilde{m}})^{2-\gamma} + (2-\gamma)(\frac{\tilde{m}}{1+\tilde{m}})^{3-\gamma}}{\sqrt{[1+(b^2-1)s^2][1+(c^2-1)s^2]}} ds \end{aligned} \quad (12)$$

with

$$\tilde{m}^2 = s^2 \left[x^2 + \frac{y^2}{1 + (b^2 - 1)s^2} + \frac{z^2}{1 + (c^2 - 1)s^2} \right]. \quad (13)$$

For $\gamma = 2$ the potential is

$$\Phi(\mathbf{r}) = \int_0^1 \frac{1/(1 + \tilde{m}) - \log[(1 + \tilde{m})s/\tilde{m}]ds}{\sqrt{[1 + (b^2 - 1)s^2][1 + (c^2 - 1)s^2]}} + C, \quad (14)$$

$$C = \int_0^1 \frac{\log t dt}{\sqrt{[1 + (b^2 - 1)t^2][1 + (c^2 - 1)t^2]}}. \quad (15)$$

The components of the force may be written

$$\begin{aligned} & \frac{\partial \Phi}{\partial x_i} \\ = & (3 - \gamma) \frac{x_i}{a_i} \int_0^1 \frac{s^2 ds}{m_i^\gamma (1 + m_i)^{4-\gamma} \sqrt{(a_i^2 + A_1 s^2)(a_i^2 + A_2 s^2)}} \end{aligned} \quad (16)$$

where

$$m_i^2(s) = s^2 \left[\frac{x^2}{a_i^2 + C_1 s^2} + \frac{y^2}{a_i^2 + C_2 s^2} + \frac{z^2}{a_i^2 + C_3 s^2} \right]. \quad (17)$$

Here we have used the notation $x_1 = x$, $x_2 = y$, $x_3 = z$, $a_1 = a$, $a_2 = b$, $a_3 = c$. The

constants in equations (16) and (17) are

$$\begin{aligned}
i = 1 : \\
& A_1 = b^2 - 1 \quad A_2 = c^2 - 1 \\
& C_1 = 0 \quad C_2 = b^2 - 1 \quad C_3 = c^2 - 1 \\
\\
i = 2 : \\
& A_1 = c^2 - b^2 \quad A_2 = 1 - b^2 \\
& C_1 = 1 - b^2 \quad C_2 = 0 \quad C_3 = c^2 - b^2 \\
\\
i = 3 : \\
& A_1 = 1 - c^2 \quad A_2 = b^2 - c^2 \\
& C_1 = 1 - c^2 \quad C_2 = b^2 - c^2 \quad C_3 = 0.
\end{aligned} \tag{18}$$

The integrals were computed by means of the double-precision FORTRAN routine DGAUSS of the CERNLIB library, which implements the classic Gaussian quadrature formula.

Hereafter we adopt units in which $G = M = a = 1$. The unit of time is $T_u = a^{3/2}/\sqrt{GM}$, or

$$T_u = 1.49 \times 10^6 \left(\frac{a}{\text{kpc}} \right)^{3/2} \left(\frac{M}{10^{11} M_\odot} \right)^{-1/2} \text{yr.} \tag{19}$$

The unit of velocity is $V_u = \sqrt{GM/a}$, or

$$V_u = 666.8 \sqrt{\frac{M/10^{11} M_\odot}{a/\text{kpc}}} \text{km s}^{-1}. \tag{20}$$

2.2. Self-consistent solutions

The magnitude of the dynamical friction force depends on the details of the stellar velocity distribution. In order to accurately follow the orbital evolution of an ejected BH, a self-consistent galaxy model is therefore required.

We constructed self-consistent triaxial models via a modification of the technique described in MF96. The densities generated by a catalogue of M orbits were recorded in a spatial grid of $N = 1008$ cells; the grid was defined as in MF96. We then sought the linear combination of orbits, with non-negative weights, which best reproduced the known mass in each cell imposing, as additional constraint, a zero streaming velocity. The quantity to be minimized was

$$\chi^2 = \frac{1}{N} \sum_{l=1}^N \left(D_l - \sum_{i=1}^m C_i B_{il} \right)^2. \tag{21}$$

In this expression, C_i is the (unknown) number of stars on orbit i ($1 \leq i \leq M$); B_{il} is the mass which the i th orbit places in the l th cell; and D_l is the (known) mass which the model places in the l th cell. The constraints $C_i \geq 0$ were also imposed, i.e., the number of stars on each orbit was required to be positive. We used the NAG quadratic-programming routine E04NCF to carry out the minimization.

We solved the self-consistency problem for the case $\gamma = 1$, a “weak” density cusp, and $\gamma = 2$, a “strong” cusp. In the $\gamma = 1$ case, we built two models with different axis ratios, as reported in Table 1. All models have a “triaxiality index” $T = 0.5$, where $T \equiv (a^2 - b^2)/(a^2 - c^2)$; i.e. they are “maximally triaxial”. The weak-cusp model is similar in structure to bright elliptical galaxies and bulges, those having absolute visual magnitudes brighter than $M_V \approx -21$, while the strong-cusp model is similar to low-luminosity spheroids like that of the Milky Way and M32, which have higher-density nuclei. Table 1 also gives, as useful reference time, the crossing time $T_{1/2}$, defined as the period of the circular orbit at the radius containing one-half of the total galaxy mass, in the “equivalent” spherical model; the latter is defined as the spherical model with scale length given by $(abc)^{1/3}$ and the same total mass.

In order to construct the velocity dispersion tensor, which is needed in the computation of the dynamical friction force, we also stored the velocities of the orbits as they passed through the cells. The velocity dispersion tensor is (Merritt 1980)

$$\sigma_{jk,l}^2 = \frac{\sum_{i=1}^N C_i B_{il} \langle V_{jk}^2 \rangle_{il}}{\sum_{i=1}^N C_i B_{il}} \quad (22)$$

where

$$\langle V_{jk}^2 \rangle_{il} = \langle V_j V_k \rangle_{il} - \langle V_j \rangle_{il} \langle V_k \rangle_{il}; \quad (23)$$

here j, k refer to the coordinate axes, i is the orbit number, and l is the cell number. The principal components of the velocity dispersion tensor, σ_k^2 , $k = 1, 2, 3$, in each cell could then be computed via standard techniques.

The high-energy cutoff in the orbital sample together with the unavoidable limitation in abundance of the orbital catalog implies that the outermost region of the spatial grid is not well populated, so we excluded from our evaluation of $\sigma_{jk,l}^2$ the 48 cells of the outermost spatial shell.

Figure 1 shows the radial behavior of the principal components of the velocity dispersion tensor in each of the three self-consistent models.

Table 1.

Model	γ	b/a	c/a	$T_{1/2}$
1	1	0.7906	0.5	21.0
2	1	0.8631	0.7	25.9
3	2	0.8631	0.7	6.91

Table 2.

ID	γ	r_c/r_{BH}^a	Core ^b	v_e^c	$v_{e,eff}/v_e^d$
1a	1	0	I	1.625	1.018 – 1.044
1d	1	0.2	II	1.620	1.008 – 1.036
1e	1	2	II	1.605	1.001 – 1.023
1f	1	0.2	III	1.620	1.008 – 1.030
1g	1	2	III	1.605	1.001 – 1.017
2a	1	0	I	1.530	1.030 – 1.047
2d	1	0.2	II	1.530	1.012 – 1.028
2e	1	2	II	1.515	1.004 – 1.019
2f	1	0.2	IV	1.530	1.009 – 1.024
2g	1	2	IV	1.515	1.004 – 1.013
3b	2	0.2	III	4.66	1.73 – 2.15
3c	2	2	III	4.04	1.89 – 2.24
3d	2	0.2	II	4.66	2.20 – 3.20
3e	2	2	II	4.04	1.11 – 1.35
3f	2	0.2	III	4.66	1.08 – 1.21
3g	2	2	III	4.04	1.00 – 1.05

^aCore radius in units of r_{BH} (Eq. 29).

^bScheme for treatment of central forces (see §2.2).

^cCentral escape velocity neglecting dynamical friction.

^dCentral escape velocity including dynamical friction.

2.3. The dynamical friction force

The classical Chandrasekhar (1943) formula for the dynamical friction force, which assumes a homogeneous and isotropic medium, has been extended by Pesce, Capuzzo-Dolcetta & Vietri (1992) to the triaxial case, in partial analogy with the Binney’s treatment of the axysymmetric case (Binney 1977). The result is

$$\mathbf{f}_{df,t} = -\Gamma_1 \hat{\mathbf{e}}_1 - \Gamma_2 \hat{\mathbf{e}}_2 - \Gamma_3 \hat{\mathbf{e}}_3 \quad (24)$$

where $\hat{\mathbf{e}}_k$ ($k = 1, 2, 3$) are the principal components of the velocity dispersion tensor and $\Gamma_k(\mathbf{r}, \mathbf{v}, v_k) = \gamma_k(\mathbf{r}, \mathbf{v})v_k$, with v_k the component of the BH’s velocity along the $\hat{\mathbf{e}}_k$ axis. The functions $\gamma_i(\mathbf{r}, \mathbf{v})$ are given by

$$\gamma_i(\mathbf{r}, \mathbf{v}) = 2\sqrt{2\pi}\rho(\mathbf{r})G^2 \ln \Lambda (m + m_\bullet)\sigma_3^{-3} \times \int_0^\infty \frac{e^{\Sigma_{k=1}^3 - \frac{v_k/2\sigma_k^2}{\epsilon_k^2 + u}}}{(\epsilon_i^2 + u)\sqrt{\Sigma_k(\epsilon_k^2 + u)}} du. \quad (25)$$

Here, m_* is the mass of a field star, $\ln \Lambda$ is the usual Coulomb logarithm, m_\bullet is the BH mass, G is the gravitational constant, $\rho(\mathbf{r})$ is the galaxy mass density, and ϵ_k is the ratio between σ_k and the largest eigenvalue, defined to be σ_3 .

The motion of the test object (the black hole) can be strongly affected by the values of the conservative and dynamical friction forces very near the center. Both components of the force would be influenced by the motion of the test particle; for instance, displacing a BH causes the central density to drop, an effect that was ignored in the construction of the models. In the case of the dynamical friction force, the limited resolution of our triaxial models is a problem; the central cells have a size of 0.28 and 0.05 for $\gamma = 1$ and $\gamma = 2$, respectively. We adopted the following scheme to deal with these issues.

The standard Chandrasekhar (1943) formula in the so called local approximation evaluates the dynamical friction force using the values of the stellar density and velocity at the position of the test particle. In the case of a particle that is at the center of a galaxy with a steep central density profile, the local approximation clearly yields an overestimate of the actual dynamical friction force, because it does not weight properly the contributions of particles in zones surrounding the center, where the density is much smaller. To overcome this problem, Capuzzo-Dolcetta & Vicari (2006) proposed, for the case of a centrally-located test particle of mass m_\bullet , the use of a numerical evaluation of the dynamical friction integral in its complete form. The fact that the test particle is at the center is exploited by identifying

the distance to the scatterer (r) with the impact parameter b , yielding

$$\mathbf{f}_{df} = -4\pi \frac{m}{m_{\bullet} + m} \times \int_{b_{min}}^{b_{max}} \int_{\mathbf{v}} f(b, \mathbf{v}) \frac{(\mathbf{v}_{\bullet} - \mathbf{v})|\mathbf{v} - \mathbf{v}_{\bullet}|}{1 + \frac{b^2|\mathbf{v} - \mathbf{v}_{\bullet}|^4}{G^2(m_{\bullet} + m)^2}} d^3\mathbf{v} db \equiv -G(v_{\bullet}) \frac{\mathbf{v}_{\bullet}}{v_{\bullet}}, \quad (26)$$

where $f(\mathbf{r}, \mathbf{v})$ is the distribution function of the background particles (of mass m) that provide the frictional force. The integral in (26) is numerically performed assuming $b_{min} = 0$ and, for b_{max} , a value large enough to guarantee convergence.

After fitting with a suitable analytic expression the numerical $G(v_{\bullet})$, we obtain an estimate of the dynamical friction force in the inner ($m \leq \bar{m} \equiv 0.05$) region of the galaxy by means of the interpolating formula

$$\mathbf{f}_{df} = -p(m)G(v_{\bullet}) \frac{\mathbf{v}_{\bullet}}{v_{\bullet}} + [1 - p(m)]\mathbf{f}_{df,t}(\bar{x}, \bar{y}, \bar{z}), \quad (27)$$

where $p(m)$ is a regular weighting function, satisfying $p(0) = 1$ and $p(\bar{m}) = 0$. The expression 27 connects the central dynamical friction force, equation (26), with its values at $m > \bar{m}$, obtained via equation (24). Here, $\bar{x}(t), \bar{y}(t)$ and $\bar{z}(t)$ are the coordinates of the intersection point between the radial direction through the position of the test particle at time t and the $m^2 = \bar{m}^2$ ellipsoidal surface (Figure 2). In the following, we assumed for simplicity a linear dependence of $p(m)$ on m .

So far, we have ignored the influence of the BH and its motion on the distribution of mass in the galaxy. In reality, sudden removal of the BH from its central location will cause the stellar density to drop. The ejected BH will carry with it stars initially contained within a region $r < r_{eff}$ such that the orbital velocity around the BH is equal to V_{kick} , or

$$r_{eff} \approx \frac{Gm_{\bullet}}{V_{kick}^2} \approx r_{BH} \left(\frac{V_{kick}}{\sigma} \right)^{-2}, \quad (28)$$

with

$$r_{BH} \equiv Gm_{\bullet}/\sigma^2 \quad (29)$$

the BH gravitational influence radius. Removal of the BH also reduces the gravitational force that binds the stars at $r \gtrsim r_{BH}$, causing them to move outward. Both effects result in a lowering of the density at $r \lesssim r_{eff}$.

A self-consistent treatment of this expansion would require N -body techniques. Here, we account approximately for the expansion by considering the dependence of our results on different assumptions about the inner form of the stellar density profile. We introduce

a “core” radius r_c , parametrized in terms of r_{BH} as $r_c = \alpha r_{BH}$, $\alpha = (0.2, 2)$. In computing r_{BH} , we set in Eq. 29 as σ the value of the velocity dispersion in the innermost model cell.

Based on these considerations, we adopted four different schemes for treating the central forces (conservative + frictional), which we denote in Table 2 via the labels I-IV. These schemes are defined as follows.

- I No modification to the density profile, i.e. $r_c = 0$. Conservative forces were computed as in equation (16) (which is possible just when the central forces are finite, i.e. $\gamma = 1$) and dynamical friction forces as in equation (27), i.e. by matching the triaxial expression to the central expression.
- II Conservative forces within the core were set to zero. Frictional forces in this region were computed via equation (24), assuming for the coefficients Γ_k their values at the boundary $r = r_c$, as averaged over angles, and with the correct velocity dependence, i.e. $\Gamma_k = \langle \Gamma_k(r_c, \mathbf{v}, v_k) \rangle_{\theta, \phi}$.
- III Density was set to zero within the core, thus conservative forces zero therein, and frictional forces in the core were evaluated setting $b_{min} = r_c$ and $p(m) = 1$ in equation (27).
- IV The density was given a core of radius r_c and the potential within the core was assumed harmonic (linear forces), matching the external triaxial potential at the core boundary. Frictional forces were computed as in I.

In what follows, we assumed a BH mass of $m_\bullet = 10^{-3}$ in units of the galaxy mass, close to the mean ratio observed in real galaxies (Merritt & Ferrarese 2001; Marconi & Hunt 2003). The Coulomb logarithm was set to $\ln \Lambda = 6.6$ (Spinnato et al. 2003). Dynamical friction times scale linearly with $(m_\bullet \ln \Lambda)^{-1}$.

3. Results

We studied the orbital evolution of the massive particle (BH) after being ejected from the center of each of the galaxy models in Table 2 with different kick velocities V and angles (θ, ϕ) , where $V_x = V \sin \theta \cos \phi$, $V_y = V \sin \theta \sin \phi$, $V_z = V \cos \theta$. The kick velocity V was assigned a value in the range $0.2v_e \leq V \leq v_{e,eff}$, where v_e is the escape velocity from the origin in the absence of frictional forces, and $v_{e,eff}$ is the actual velocity required for escape; $v_{e,eff} > v_e$ since dynamical friction acts to reduce the particle’s kinetic energy. Table 2 gives v_e and $v_{e,eff}/v_e$ (the latter expressed as a range, since $v_{e,eff}$ depends on the launching angle) for each of the models. The direction of the kick was given one of 43 values by choosing θ and ϕ from the discrete set $(0^\circ, 15^\circ, 30^\circ, 45^\circ, 60^\circ, 75^\circ, 90^\circ)$. We defined the decay time T_{df} as the time when the BH orbital energy had dropped to 1% its initial value and its residual time variation was negligible ($|\dot{E}/E_0| \leq 10^{-4}$).

Figures 3 and 4 show the evolution of a representative set of orbits. Figure 3 shows that for moderate kicks ($V \lesssim 0.4v_e$) the BH executes only one “bounce” before dynamical friction brings it to a halt at the center. Figure 4 illustrates some higher energy orbits ($V/v_e = 0.8, 0.9$) in a strong-cusp model ($\gamma = 2$). In spite of the strong frictional forces near the center of this model, ejection with a sufficiently large V allows the BH to execute several oscillations before coming to rest.

The dependence of the effective escape velocity $v_{e,eff}$ on launching angle for two galaxy models is illustrated in Figure 5. The increase in $v_{e,eff}$ relative to v_e is most striking for trajectories aligned with the x – (long) axis, and in models with high central densities ($\gamma = 2$); $v_{e,eff}/v_e$ can be as large as ~ 3 (Table 2). However, Table 2 also shows that $v_{e,eff}/v_e$ for these high density models can depend substantially on how the central forces are treated. For this reason, we consider the largest values of $v_{e,eff}/v_e$ in Table 2 to be provisional, until they can be verified with detailed N -body simulations.

Figures 6-9 show the dependence of the decay time, T_{df} , and of the apocentric “ellipsoidal” distance, m_{max} , on the initial velocity in four of the models, for the entire set of launching angles. For the sake of comparison, the values of T_{df} and m_{max} for the “equivalent” spherical model, characterized by the density law (6) with r instead of m and length scale equal to $(abc)^{1/3}$, are plotted as dotted lines. Kicks along the symmetry axes result in the shortest return times: the corresponding orbits are exactly radial and pass precisely through the dense center on each return, as in a spherical model. Return times are longer than in a spherical model, by as much as an order of magnitude in the $\gamma = 1$ models, and even larger factors in the $\gamma = 2$ models.

These figures also show that oscillations along the major axis are quenched more rapidly than along the other axes, as demonstrated previously by Capuzzo-Dolcetta & Vicari (2005). Even though orbits launched close to the z - (short-) axis reach the greatest values of m_{max} at every v/v_e , their decay times are not necessarily the longest. This is because the dynamical friction force transforms the near-radial orbit into a box orbit which has a thin waist, thinner than that of orbits having the same initial energy but launching angles $\theta \neq 0$; the dynamical friction force is therefore greater because of the closer approach of the BH to the high-density regions. This is not a trivial result, because the galactic models treated in this paper are cuspy, and it was not *a priori* obvious that the large-scale behavior of the density would exert the dominant influence on the motion. At first sight it is surprising that the oscillations in the equivalent spherical models are always shorter than in the triaxial case. since in absence of dynamical friction, the radial oscillation in the spherical case reaches a maximum extension which is intermediate between the displacements along the x and z axes in the triaxial case. However, the return time is always shortest in the spherical geometry since the effect of dynamical friction in the triaxial case is progressively greater from x to z , making the x oscillation the shortest, but still larger than in the spherical case.

Decay times are often of the same order, or less than, the period of an unperturbed radial

orbit in the spherical geometry, particularly in the models with $\gamma = 2$. This is illustrated in Figure 10 for two models. Thus, in many cases, a kicked BH executes only \sim one or fewer complete radial oscillations before coming to rest.

Figure 11 illustrates the dependence of T_{df} on the launching angle. Decay times peak for intermediate angles, as was already apparent from Figures 6-9.

4. Consequences for Black Hole Displacements

While triaxiality has the effect of lengthening the mean return time of a kicked BH to the center, compared with the time in a spherical galaxy (Figs. 6-9), infall times are still typically short, of order a galaxy crossing time, unless the kick velocity is close to the escape velocity. Another way to state this result is to say that there is a narrow range of kick velocities such that the BH spends a long time away from the center without being fully ejected.

Here we estimate the probability that a kicked BH will be found at an appreciable distance from the center in a randomly-chosen galaxy. Since the distribution of kick velocities is poorly known, we will present results as a function of V/v_e . The other parameter that determines the likelihood of finding a displaced BH is the time τ since the galaxy experienced its last merger (which we equate with the elapsed time since the kick). This time is also poorly known for any galaxy. We therefore assume that τ follows a Poisson distribution,

$$p(\tau)d\tau = \frac{e^{-\tau/t_{\text{merge}}}}{t_{\text{merge}}}d\tau, \quad (30)$$

with t_{merge} the mean time between mergers.

Let $P_V(r; \Delta t)dr$ be the probability of finding a kicked BH a distance r to $r + dr$ from the center of the galaxy at a time Δt after the kick. In the case of a triaxial galaxy, we define P_V as an average over the two launch angles (θ, ϕ) . Clearly for $\Delta t \geq T_{df,V}$, this distribution is a delta function at the origin, where $T_{df,V}$ is defined to be the maximum return time for kicks of magnitude V . In a randomly-chosen galaxy, the distribution of displacements for kicks of magnitude V is

$$N_V(r) = \int_0^\infty p(\tau)P_V(r; \tau)d\tau. \quad (31)$$

We simplify this expression by assuming that T_{df} is short compared with t_{merge} , allowing us to approximate equation (31) by

$$N_V(r) \approx P_V(r) \int_0^{T_{df,V}} p(\tau)d\tau + \delta(r) \int_{T_{df,V}}^\infty p(\tau)d\tau \quad (32)$$

where $P_V(r)$ is defined as the distribution of displacements averaged over the time $0 \leq \Delta t \leq T_{df,V}$. Thus

$$N_V(r) \approx (1 - e^{-T_{df,V}/t_{\text{merge}}}) P_V(r) + e^{-T_{df,V}/t_{\text{merge}}} \delta(r) \quad (33)$$

and the cumulative distribution describing displacements less than r is

$$N_V(< r) \approx (1 - e^{-T_{df,V}/t_{\text{merge}}}) P_V(< r) + e^{-T_{df,V}/t_{\text{merge}}}. \quad (34)$$

We computed $P_V(< r)$ on a grid of V/v_e -values for several of the models, then used these numbers to compute the probability distributions $N_V(< r)$ as a function of the two parameters

$$(T_{1/2}/t_{\text{merge}}, V/v_e) \quad (35)$$

where $T_{1/2}$ is a proper reference time defined, as above (Table 1), as the period of a circular orbit at the half-mass radius ($\sim r_{1/2}$) in the equivalent spherical model. Figures 12 and 13 show the results for Models 1a and 2a; these models both have $\gamma = 1$ and no “core” (Table 2), differing only in their triaxiality (Table 1). These figures demonstrate that the probability of finding a kicked BH at a distance $\sim r_{1/2}$ from the center of a galaxy is low unless the kick velocity is high, $\gtrsim 0.8v_e$, and the mean time between mergers is not too long compared with the crossing time. Based on Figs. 6-9, this conclusion would be even stronger for models like 3b or 3c which have higher central densities.

The largest value expected for V is $\sim 200 \text{ km s}^{-1}$ in the absence of spin (González et al. 2006; Sopuerta, Yunes & Laguna 2006). By comparison, escape velocities from giant elliptical galaxies ($M_V \lesssim -18$) are always greater than $\sim 400 \text{ km s}^{-1}$ (Merritt et al. 2004). Hence the probability of finding a significant displaced supermassive BH in a bright E galaxy is very small, unless a merger occurred very recently. Escape velocities from dwarf elliptical (dE) galaxies ($-12 \lesssim M_V \lesssim -18$) are $\lesssim 150 \text{ km s}^{-1}$ if only the stellar contribution to the potential is considered, and $\lesssim 300 \text{ km s}^{-1}$ if the dark matter potential is included (Merritt et al. 2004). (Escape velocities from luminous E galaxies are dominated by the stars.) However in these galaxies the mean time between mergers is believed to be very long, again implying a low probability of finding a displaced BH.

5. Conclusions

We integrated the motion of “kicked” BHs in triaxial models of galaxies, using the expressions derived by Pesce, Capuzzo-Dolcetta & Vietri (1992) and Capuzzo-Dolcetta & Vicari (2006) for the dynamical friction force in an anisotropic stellar distribution. The velocity dispersion components were computed from fully self-consistent triaxial models, constructed via orbital superposition. We considered different possible forms for the stellar density at the center of the galaxy, since ejection of the BH would significantly affect the distribution of stars there. Our main results can be summarized as follows:

1. Dynamical friction increases the effective escape velocity from a galaxy. This effect is modest, roughly a few percent, in galaxy models with shallow central density profiles, but can be very significant in galaxies with $\rho \sim r^{-2}$ central density profiles, since the frictional force acting on the BH is so strong near the center (Table 1).

2. Since the dynamical friction force in a triaxial galaxy depends on angle as well as distance from the center, escape velocities are a function of “launching angle”, being greatest in the direction of the long axis. Again, this effect is modest in models with low central concentration but can be appreciable in galaxies with high central densities (Fig. 5).

3. The time for a kicked BH to return to the center with zero velocity is longer in a triaxial galaxy than in a spherical galaxy with the same radial density profile and length scale $(abc)^{1/3}$, and when kicked with the same fraction of the escape velocity. The main reason is that trajectories in the triaxial geometry are not linear (unless they are exactly along the coordinate axes) and a kicked BH does not return precisely through the center, thus reducing the average dynamical friction force (Figs. 3, 4). Infall times are typically several times longer than in the spherical geometry (Figs. 6-9).

4. In spite of the delaying effects of the triaxial geometry, BHs with masses similar to those observed in real galaxies ($M \approx 10^{-3}M_{gal}$) return to the center in less than \sim a galaxy crossing time, unless the kick velocity is a large fraction of the escape velocity. Since escape velocities in giant elliptical galaxies are large compared with the maximum kick velocities so far computed by numerical relativists, the chance of finding a BH substantially displaced from the center of such a galaxy is small (Figs. 13, 14). Escape velocities are smaller in dE galaxies but the mean time between mergers is probably long, again implying a small probability of finding a displaced BH.

DM acknowledges support from grants AST-0206031, AST-0420920 and AST-0437519 from the NSF, grant NNG04GJ48G from NASA, and grant HST-AR-09519.01-A from STScI. This work was supported in part by the Center for Advancing the Study of Cyberinfrastructure at the Rochester Institute of Technology.

REFERENCES

- Baker, J. G., Centrella, J., Choi, D.-I., Koppitz, M., & van Meter, J. R. 2006a, PRL 96, 111102
- Baker, J. G., Centrella, J., Choi, D.-I., Koppitz, M., & van Meter, J. R. 2006b, PRD, 73, 104002
- Baker, J. G., Centrella, J., Choi, D.-I., Koppitz, M., van Meter, J. R., & Miller, M. C. 2006c, ArXiv Astrophysics e-prints, arXiv:astro-ph/0603204

- Bekenstein J.D. 1973, ApJ, 183, 657
- Binney J., 1977, MNRAS, 181, 735.
- Blanchet, L., Qusailah, M. S. S., & Will, C. M. 2005, ApJ, 635, 508
- Boylan-Kolchin M., Ma C. & Quataert E. 2004, ApJ, 613, L37
- Campanelli, M. 2005, Classical and Quantum Gravity, 22, 387
- Campanelli, M., Kelly, B., & Lousto, C. O. 2006a, Phys. Rev. D, 73, 064005
- Campanelli, M., Lousto, C. O., Marronetti, P., & Zlochower, Y. 2005, PRL, 96, 111101
- Campanelli, M., Lousto, C. O., & Zlochower, Y. 2006, Phys. Rev. D, 74, 084023
- Campanelli, M., Lousto, C. O., & Zlochower, Y. 2006, Phys. Rev. D, 74, 041501
- Capuzzo-Dolcetta R., Vicari A., 2005, MNRAS, 356, 899
- Capuzzo-Dolcetta R., Vicari A., 2006, in preparation
- Chandrasekhar S. 1943, ApJ, 97, 255
- Chandrasekhar S. 1969, Ellipsoidal Figures of Equilibrium, New Haven, Yale University Press
- Dehnen W. 1993, MNRAS, 265, 250
- Favata M., Hughes S.A., Holz D.E. 2004, ApJ, 607, L5
- Fehlberg, E. 1968, NASA Tech. Rep. TR R-287
- Fitchett, M. J. 1983, MNRAS, 203, 1049
- Fitchett, M. J., & Detweiler, S. 1984, MNRAS, 211, 933
- Haiman, Z. 2004, ApJ, 613, 36
- Herrmann, F., Shoemaker, D., & Laguna, P. 2005, ArXiv e-prints, arXiv:gr-qc/0601026
- Libeskind, N. I., Cole, S., Frenk, C. S., & Helly, J. C. 2006, MNRAS, 368, 1381
- Madau, P., & Quataert, E. 2004, ApJ, 606, L17
- Marconi, A., & Hunt, L. K. 2003, ApJ, 589, L21
- Merritt, D. 1980, ApJS, 43, 435
- Merritt D., Fridman T. 1996, ApJ, 460, 136.

- Merritt, D., & Ferrarese, L. 2001, MNRAS, 320, L30
- Merritt D., Milosavljevic M., Favata M., Hughes S.A., Holz D.E. 2004, ApJ, 607, L9
- Moncrief V. 1980, ApJ, 238, 333
- Nakamura, T., Oohard, K., & Kojima, Y. 1987, Prog. Theor. Phys. Supl., 90, 1
- Pesce E., Capuzzo-Dolcetta R., Vietri M. 1992, MNRAS, 254, 466.
- Pretorius, F. 2005, Physical Review Letters, 95, 121101
- Pretorius, F. 2006, ArXiv General Relativity and Quantum Cosmology e-prints, arXiv:gr-qc/0602115
- Redmount, I.H, Rees, M.J. 1989, Com. Ap., 14, 165
- Schwarzschild, M. 1979, ApJ, 232, 236
- Spinnato P.F., Fellhauer M., Zwart S.F.P. 2003, MNRAS, 344,22.
- Volonteri, M., Haardt, F., & Madau, P. 2003, ApJ, 582, 559
- Wiseman, A. G. 1992, Phys. Rev. D, 46, 1517
- Yoo, J., & Miralda-Escudé, J. 2004, ApJ, 614, L25

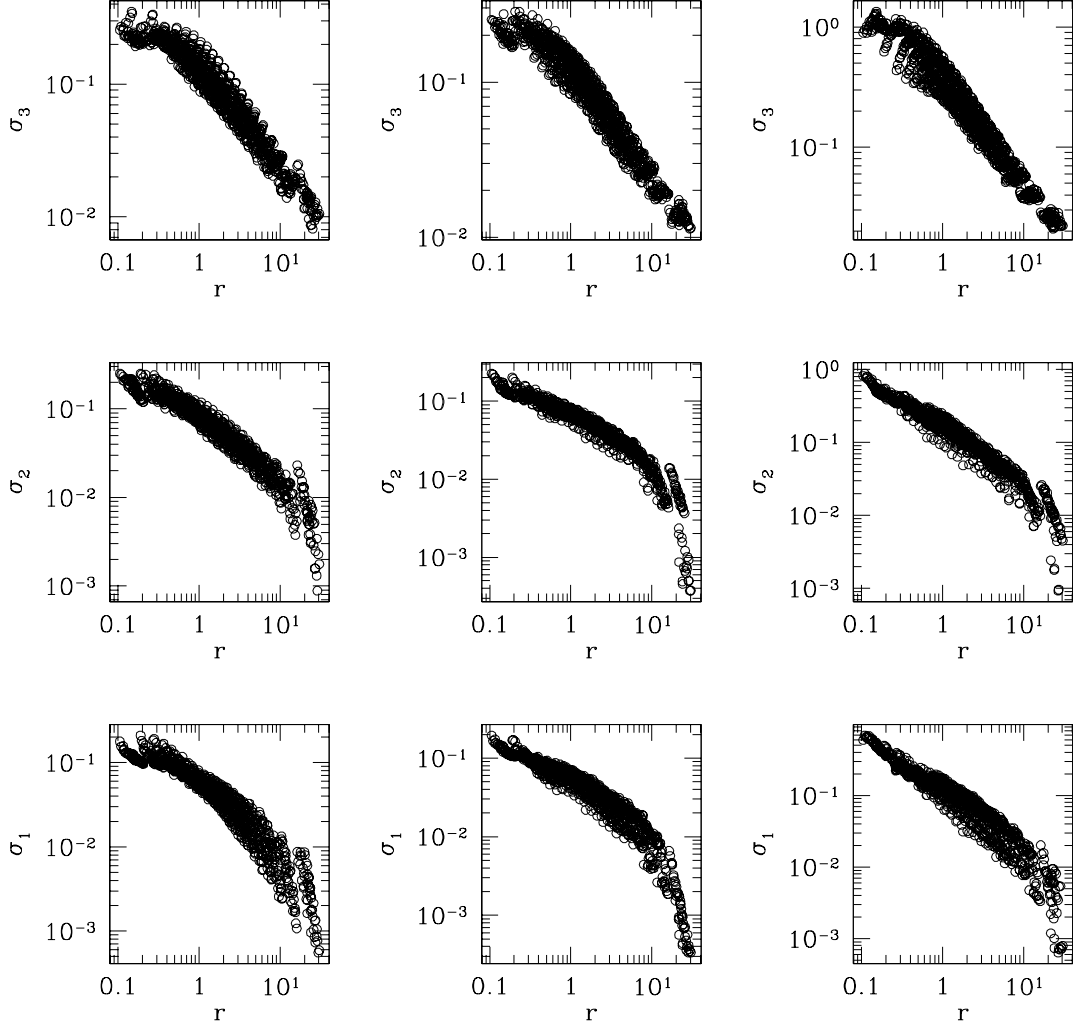


Fig. 1.— The radial behavior of the principal components of the velocity dispersion tensor in the three self-consistent models. The left column refers to model 1, the central column to model 2 and the right column to model 3 (see Table 1).

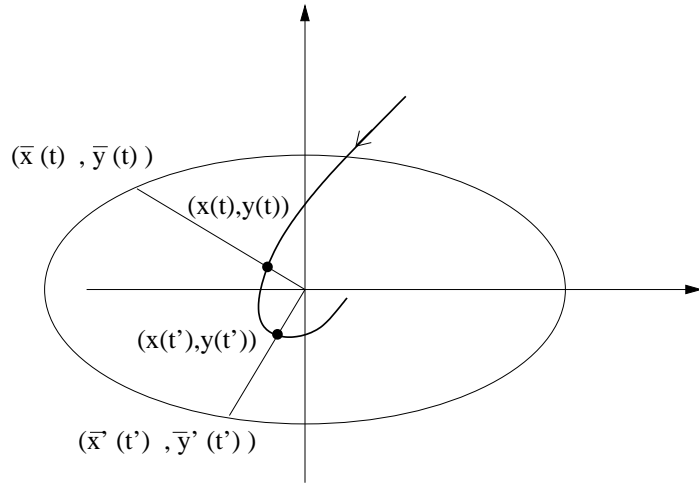


Fig. 2.— A two-dimensional illustration of the definition of \bar{x} and \bar{y} ; the solid curve is the orbit of the BH. The ellipse has equation $m^2 = \bar{m}^2$.

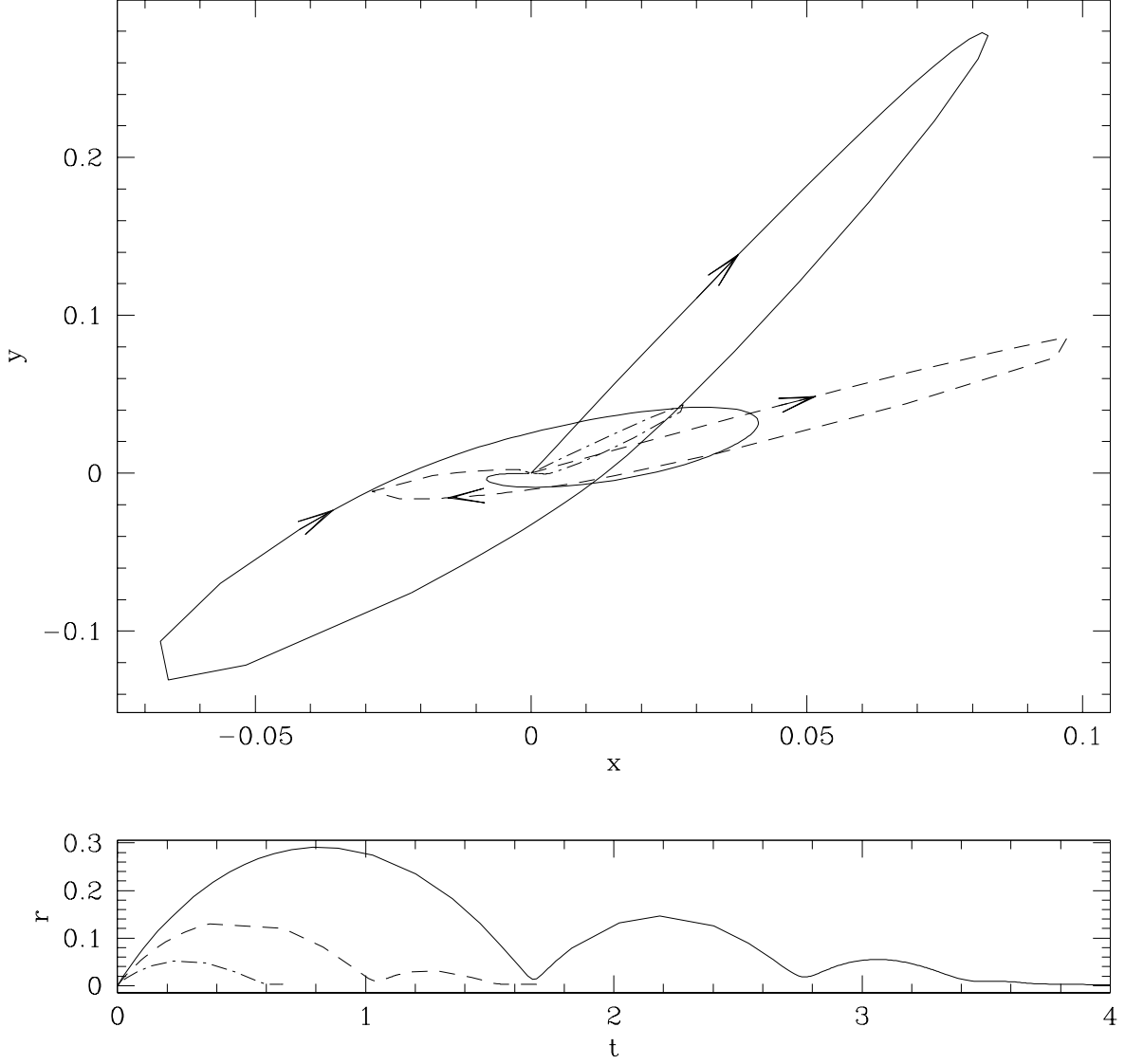


Fig. 3.— Evolution of three planar ($x = 0$) orbits in model 2a ($\gamma = 1$), for $V/v_e = (0.4, 0.5, 0.6)$; for display convenience, we chose orbits with a different initial θ . Arrows indicate the direction of the motion for the two more energetic orbits. The lower panel shows the distance of the BH from the center as function of time.

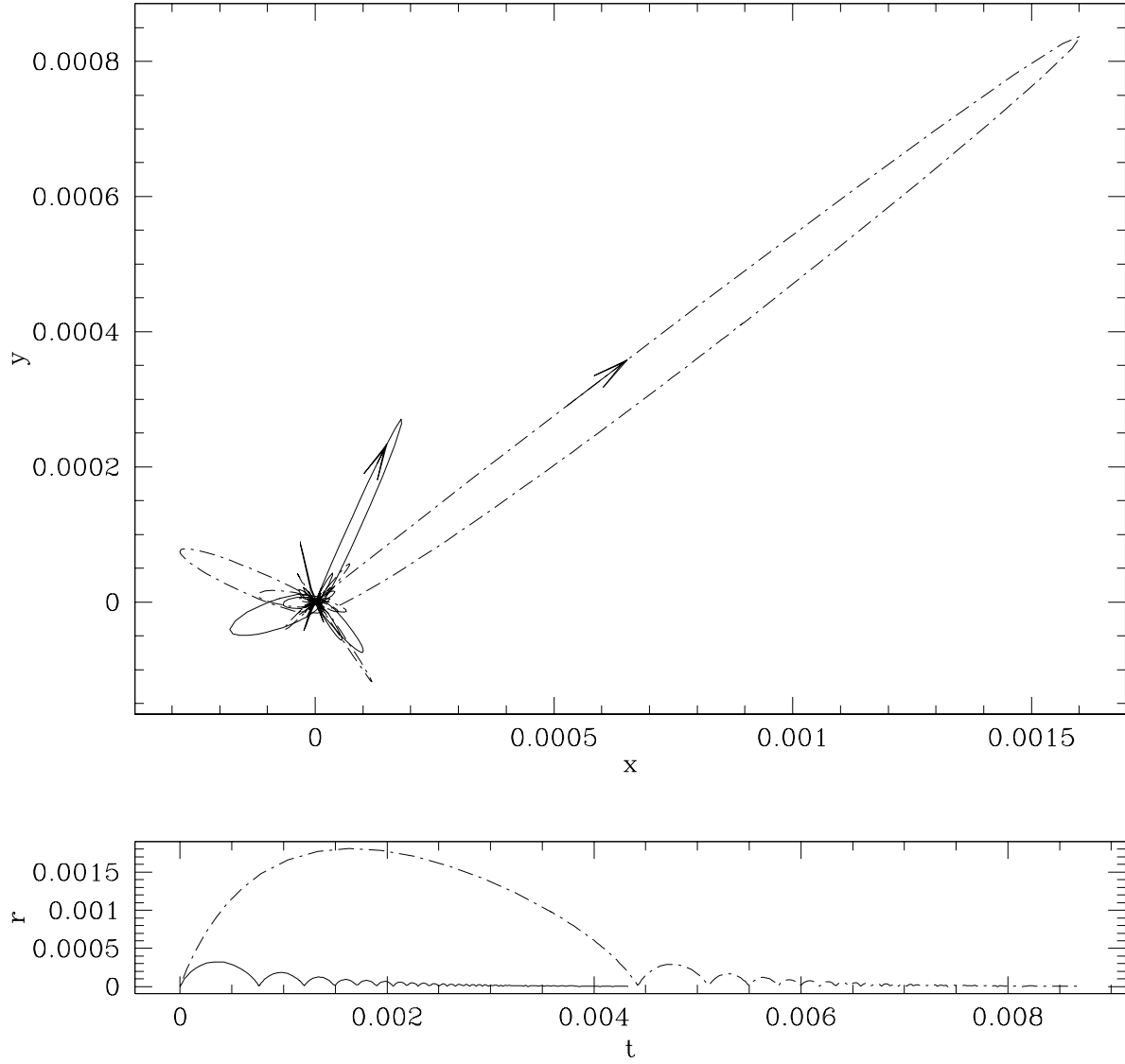


Fig. 4.— As in Figure 3, for two planar orbits in model 3b ($\gamma = 2$), with $V/v_e = (0.8, 0.9)$.

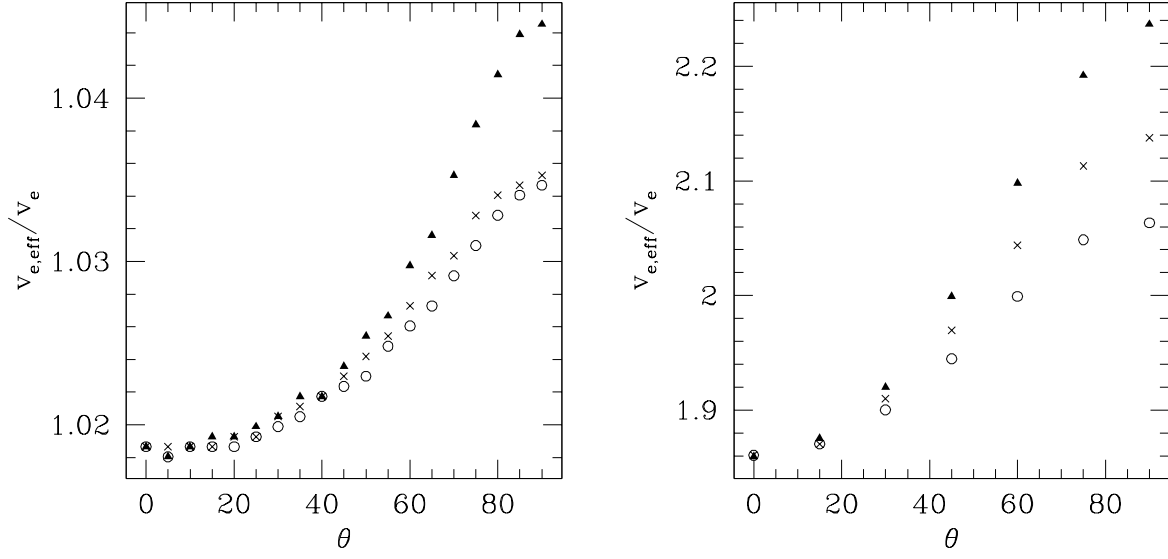


Fig. 5.— Effective escape velocity as function of launching angle θ , for model 1a (left panel) and 3c (right panel). Empty circles refer to $\phi = 90^\circ$, crosses to $\phi = 45^\circ$, and black triangles to $\phi = 0^\circ$.

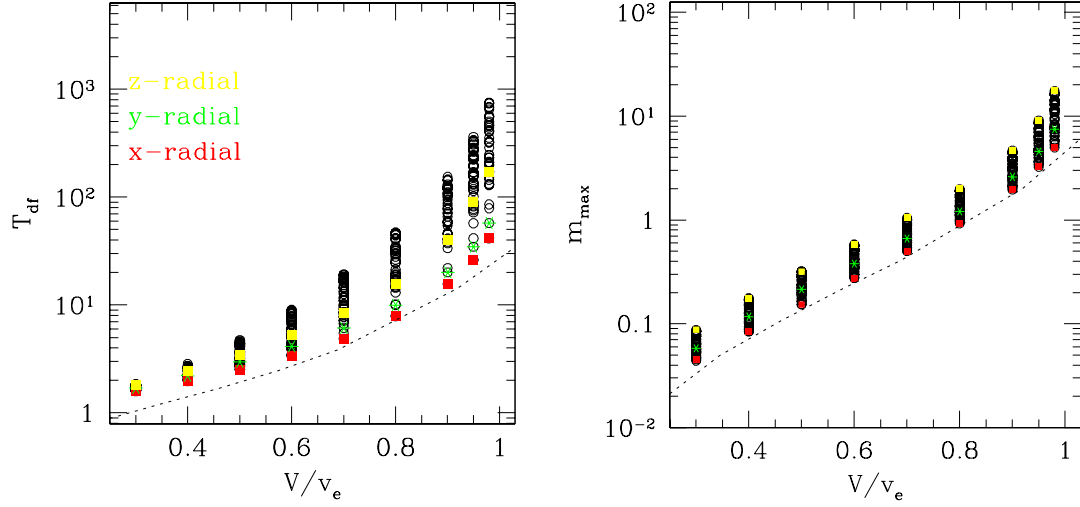


Fig. 6.— *Left panel:* Decay time T_{df} of the BH as function of the kick velocity V and for several launching angles. *Right panel:* the maximum displacement of the BH. In both panels, dotted lines are for the “equivalent” spherical model, with scale length $(abc)^{1/3}$. All results in this figure refer to model 1a.

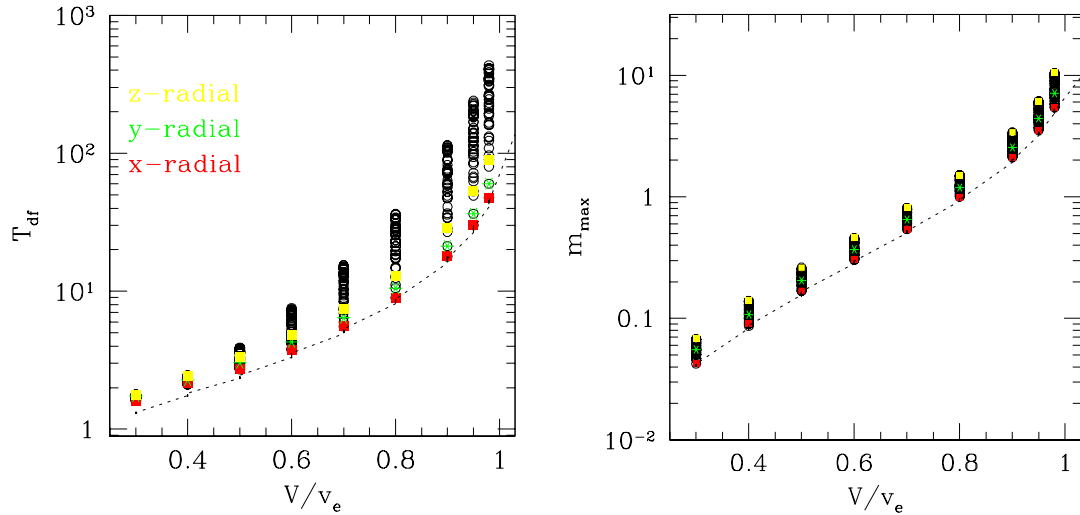


Fig. 7.— Like Figure 6, but for model 2a.

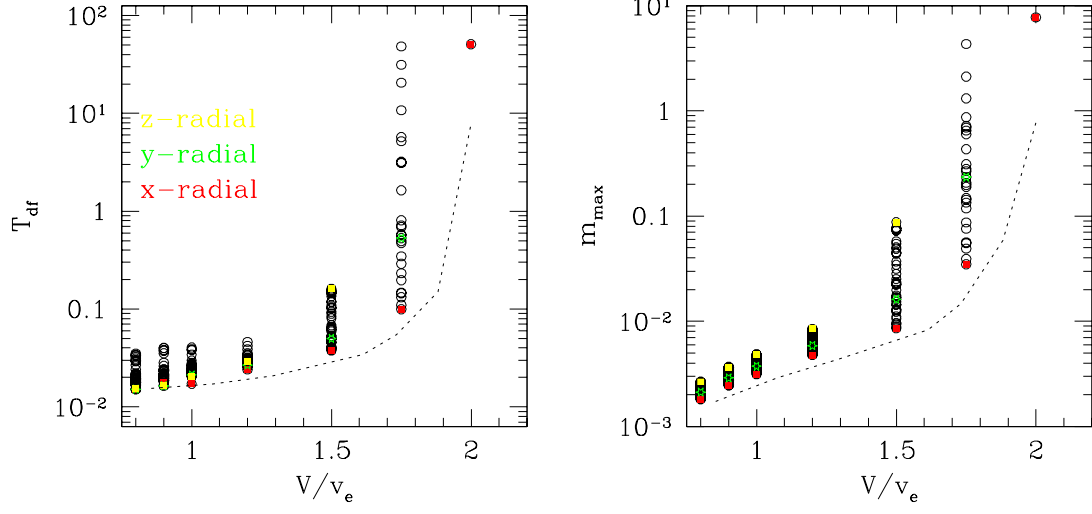


Fig. 8.— Like Figure 6, but for model 3b.

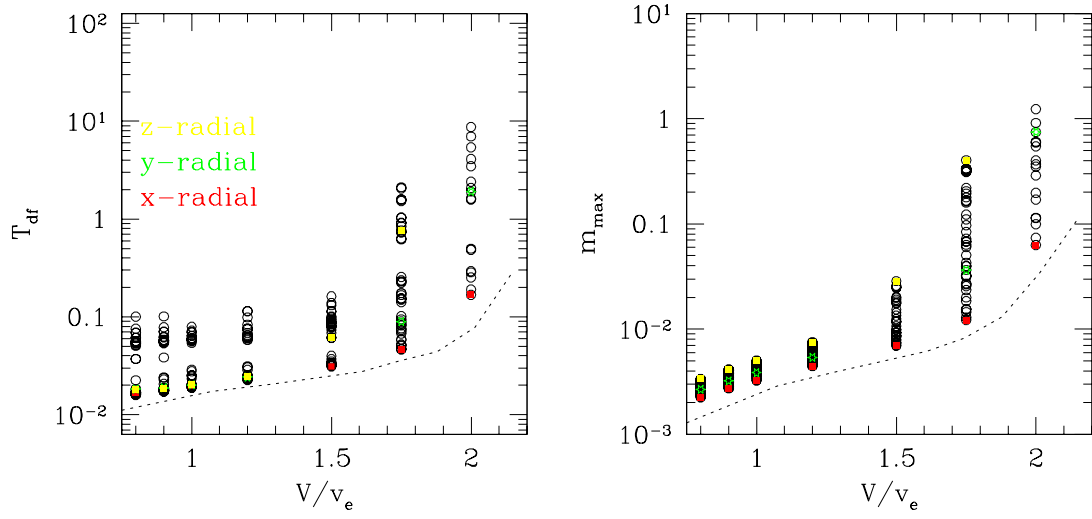


Fig. 9.— Like Figure 8, but for model 3c

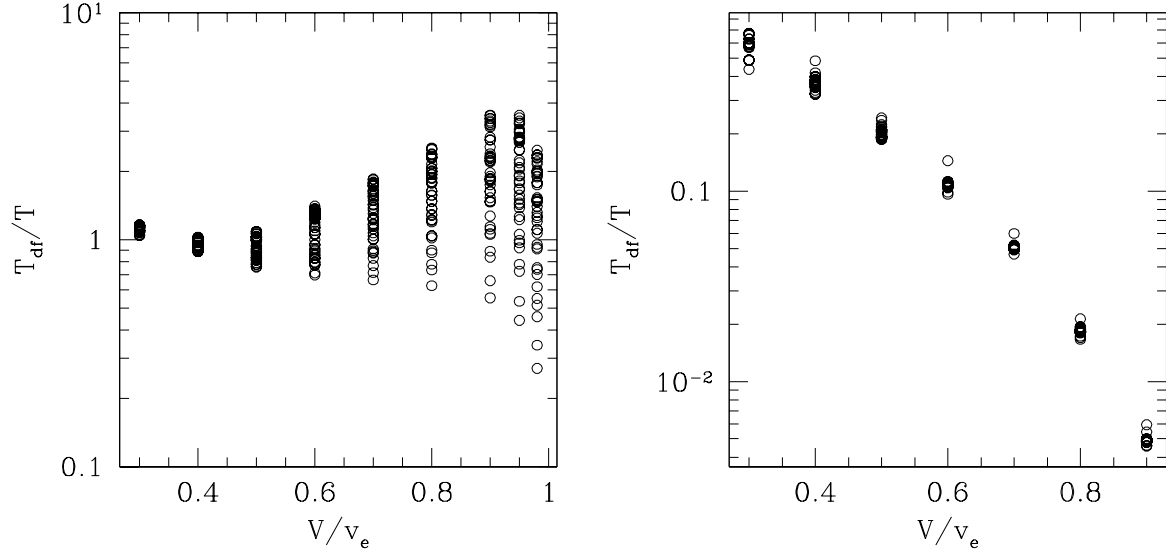


Fig. 10.— Orbital decay time in units of the period T of the unperturbed x -axial orbit of the same energy, for models 2a (left panel) and 3b (right panel).

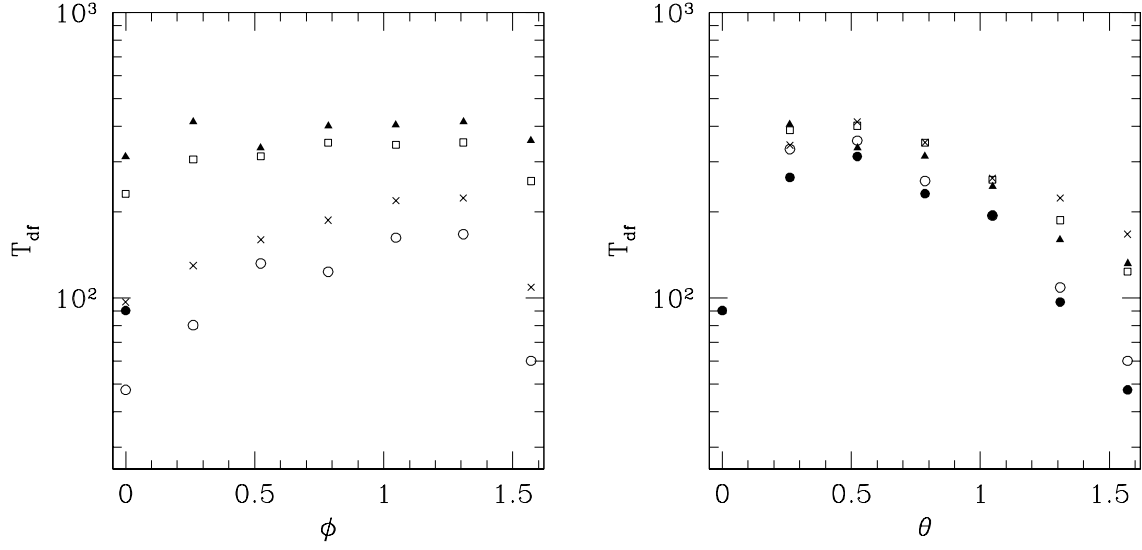


Fig. 11.— Orbital decay times in model 1a as a function of launching angle ϕ (left panel) and θ (right panel), for $v_0/v_e = 0.8$. In each panel, symbols of the same type represent fixed values of the other angle, according to the scheme: black circles = 0° ; black triangles = 30° ; squares = 45° ; crosses = 75° ; empty circles = 90° .

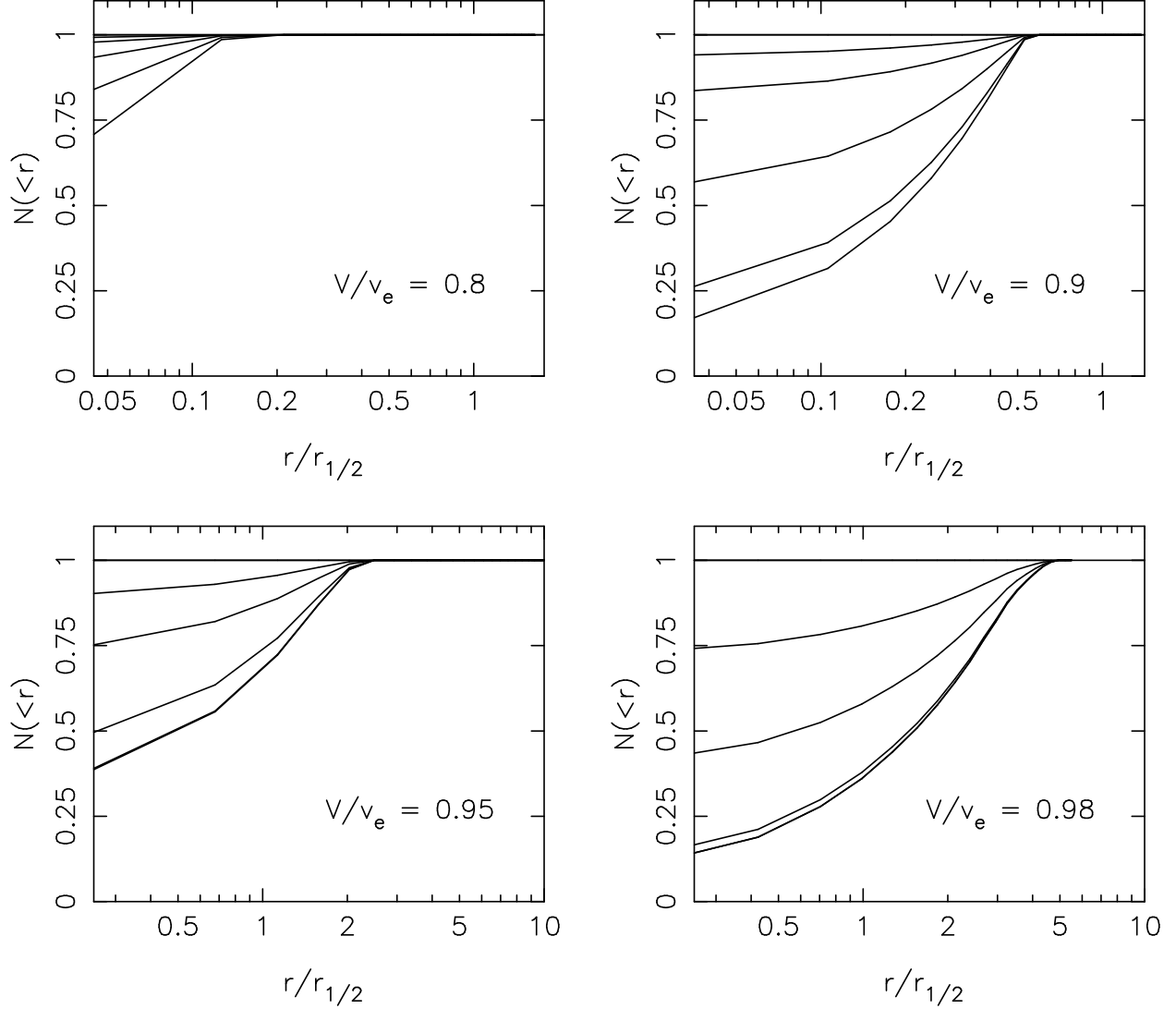


Fig. 12.— Cumulative distributions $N_V(<r)$ for the model 1a, for four different values of V/v_e . Each frame plots equation (34) for four different values of $T_{1/2}/t_{merge}$, where $T_{1/2}$ is the period of a circular orbit at the half-mass radius in the equivalent spherical model, and t_{merge} is the mean time between galaxy mergers, i.e. between kicks. The values of $T_{1/2}/t_{merge}$ are (0, 0.01, 0.03, 0.1, 0.3, 1); when this ratio is zero, the cumulative distribution is a step-function, i.e. the BH would have returned to the origin.

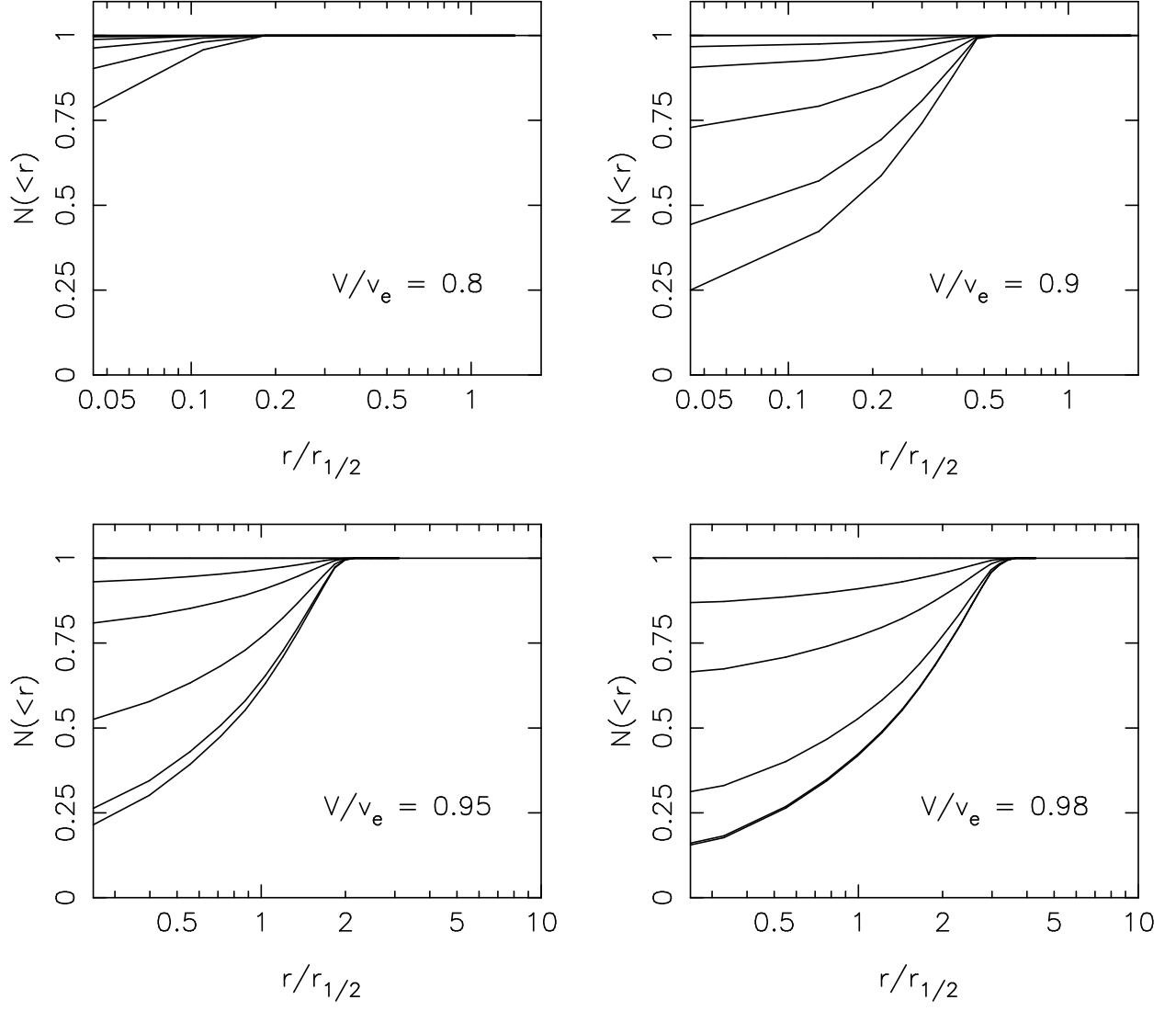


Fig. 13.— Like Fig. 12 but for model 2a.